Applied Physics A (2018) 124:281
https://doi.org/10.1007/s00339-018-1645-y

Applied Physics A
Materials Science & Processing

Phase gradient metasurface with broadband anomalous reflection based on cross-shaped units

Zhaobin Chen[1] · Hui Deng[1] · Qingxu Xiong[1] · Chen Liu[2]

Received: 13 September 2017 / Accepted: 2 February 2018

Abstract
It has been pointed out by many documents that a phase gradient metasurface with wideband characteristics can be designed by the unit with a low-quality factor (Q value). In this paper, a cross-shaped unit with a low-quality factor Q is proposed. By changing the variable parameters of the unit, it is found that the reflection phase of the unit can achieve a stable distribution of phase gradient in the frequency range of 8.0–20.0 GHz. we analyze variation of the electromagnetic field distribution on the unit with frequency and find that the size along electrical field polarization of electromagnetic field distribution area changes with frequency. Based on our design, effective size of electromagnetic field distribution area keeps meeting the subwavelength condition, thus stable phase distribution is gained across broadened bandwidth. It is found by the analysis of the phase gradient metasurface composed of seven units that the metasurface can exhibit anomalous reflection in the wide frequency band of 8.0–20.0 GHz, and the efficiency of abnormal reflection is higher in the range of 10.0–18.0 GHz. The error between the simulation results of abnormal reflection angle and the theoretical result is only − 1.5° to 0.5° after the work of comparison. Therefore, the metasurface designed by the new cross-shaped unit has a good control on the deflection direction of the reflected wave, and shows obvious advantages in widening the bandwidth.

1 Introduction

Metamaterial is a composite or structured material that exhibits properties not found in naturally occurring materials or compounds. Since the bandwidth of a traditional metamaterial itself is relatively narrow, relatively thick [1–3], its application is limited. Many scholars have tried to broaden bandwidth and reduce the thickness. Metasurface is one kind of ultra-thin metamaterial. In 2011, Capasso et al. used V-shaped antenna structures to design metasurfaces with phase gradient, and studied a series of interesting optical phenomena such as anomalous reflection and refraction. At the same time, the generalized reflection and refraction laws were deduced and confirmed experimentally. The results show that the additional gradient phase shift along propagation path of light can provide great flexibility in molding optical wavefront. It breaks the constraint of standard optical components, which rely on gradual phase accumulation along the optical path to change the wavefront of propagating light [4]. Subsequently, many studies on metasurface of scholars have shown that the metasurface has potential application in many Aspects. For example: realization of phenomenon of anomalous reflection and refraction [5–8]. Through a reasonable design, it can be used as a waveform conversion device [9–11] and be used as a non-aberration flat lens for high numerical aperture lenses [12]. It can also be used to reduce the back RCS [13–16] and so on. In many applications, the metasurface has the advantages of small physical space and less energy loss, and can exhibit similar functions as the three-dimensional metamaterial, so that the metasurface can be used instead of the three-dimensional metamaterial [17]. Because the metasurface not only has the unique three-dimensional metamaterial unique electromagnetic properties, but also has a thin, easy processing, easy to form a unique advantage [18]. Professor Barnes of the University of Exeter in England rated the technology most likely to be used in the first generation of practical nanophoton functional devices [19].

From the appearance of metasurface's concept to the present, scholars have been trying to find the way to broaden the metasurface bandwidth. Initially, scholars used V-shaped

✉ Zhaobin Chen
zbin0808@163.com

[1] School of Electronics and Information Engineering, Beihang University, Beijing 100191, China

[2] School of Sino-French Engineer, Beihang University, Beijing 100191, China

Published online: 02 March 2018

antenna structure to design metasurfaces, and observed abnormal reflection and refraction phenomenon, but the bandwidth is only 1.0–1.9 μm [20]. To solve this problem, Yongfeng Li et al. proposed a reflective metasurface, making the metasurface bandwidth to be widened [21]. In [22], 90% transmission efficiency and 99% polarization conversion efficiency can be realized based on the generalized Huygens principle, with a superposition of the scattering contributions from several electric and magnetic multipolar modes of the constituent meta-atoms, to achieve destructive interference in reflection over a large spectral bandwidth. Yang et al. utilize multiple reflections within the poly (methyl methacrylate) spacer layer to smooth the phase variation, resulting in polarization conversion rate above 98% over broadband (200 nm) [23]. In paper of Yu et al. Si-nanoparticles is utilized to create strong Mie-type scattering resonances when the refractive index of the dielectric material is sufficiently high (e.g., > 2) within visible and near-infrared range. On the condition that simultaneous excitation and mutual interference of magnetic and electric-dipole resonances in the nanodisks occur, the nanodisks array exhibits very high transmission characteristics. In addition, it is mentioned that some geometries have significantly greater overlap of electric and magnetic-dipole resonances, resulting in high transmission characteristics across a relatively broad spectral bandwidth [24]. In [25] Shulin Sun proposed to use the strong coupling of near field between the metal patch and the ground plane to produce a magnetic resonators response to the electromagnetic wave and achieve an metasurface with efficient, broadband anomalous reflection that can work at 750–900 nm in the shorter wavelength range. In [26], to solve the problem of narrow bandwidth, the resonant strength of the element is reduced by increasing the thickness of the intermediate medium, but the reflection phase of the element cannot completely cover 0–2π. To make the phase uniformly distributed in the range of 0–2π, an additional sheet with gradient refractive index is added to the upper surface of low Q value, so that the bandwidth of abnormal reflection of the metasurface is 4 GHz. For the wider applications of metasurface, it is necessary to broaden the bandwidth.

This paper presents a cross-shaped unit for the design of metasurface with wide bandwidth of anomalous reflection. It can be seen from the analysis results of the unit that the unit has a reflectance of more than 97% in the frequency range of 8.0–20.0 GHz, and a phase shift of approximate 2π can be achieved by changing the geometric parameters of the unit. As the new unit can meet the subwavelength conditions both in high and low frequency band, it is ensured that the design of the phase gradient metasurface has a wider bandwidth. Compared with the phase gradient metasurface in [26], the metasurface designed in this paper does not need to add another dielectric layer, and the relative bandwidth of the metasurface is increased to more than 85% and the absolute bandwidth is 12 GHz. Phase gradient metasurface we designed exhibits anomalous reflection over a wider frequency band than that in [27].

2 Design of metasurface

2.1 Analysis of electromagnetic characteristics of metasurface units

For the metasurface units of the equivalent circuit type, although it is very similar to the periodic units of traditional metamaterials, it is not appropriate to use the electromagnetic parameters of traditional three-dimensional metamaterial to described the metasurface electromagnetic properties because its thickness is much smaller than the wavelength and the equivalent circuit theory is used instead [28]. In the equivalent circuit theory, the equivalent impedance is determined by the combination of the distributed resistance, the distributed inductance and the distributed capacitance in the metasurface. According to the basic nature of the electromagnetic field we can see that the capacitance is determined by the electric field in the medium, and the inductance is determined by the magnitude of the current in the metal wire.

According to the literature [26] we can see that when the distance between the upper metal and the ground of the unit is relatively small, the strong resonance between the upper layer and the ground is generated under the action of the incident wave and the quality factor Q is relatively high. Although the phase shift of 2π can be ensured by adjusting the size of the unit, the bandwidth is narrow. When the distance between the upper metal and the ground of the unit gradually increases, the resonant response between the upper metal and the ground is gradually weakened, and the quality factor Q is gradually reduced. When the distance is large, the geometrical parameters of the element can be changed to achieve a relatively stable phase shift in the wide frequency band.

Therefore, for an unit of equivalent circuit type metasurface with a low Q value, the upper metal layer of the unit can be regarded as an extremely thin impedance boundary. The impedance layer can be equivalent to the result of the interaction between the equivalent inductance L and the equivalent capacitance C. When the size of the upper metal layer of the unit is changed, the equivalent inductance L and the equivalent capacitance C of the unit are changed accordingly, thereby changing the equivalent impedance of the surface. Since the reflection phase of the element can be derived from the surface impedance, the variation of the reflection phase with the unit parameters is given in [26] as follows:

$$\theta_r = \arg\left(\frac{\left(1-\sqrt{\varepsilon_2}-Y_s/Y_0\right)-\left(1+\sqrt{\varepsilon_2}-Y_s/Y_0\right)\exp(2ikh)}{\left(1+\sqrt{\varepsilon_2}+Y_s/Y_0\right)-\left(1-\sqrt{\varepsilon_2}+Y_s/Y_0\right)\exp(2ikh)}\right), \quad (1)$$

where ε_2 and h are the dielectric constant and thickness of the dielectric layer, $Y_S = 1/Z_S$ is the equivalent admittance of the unit surface, and k is the wave vector in the dielectric layer.

From the above resonance analysis of the unit, when the unit has a weak resonant response characteristic (i.e., low Q value), it is possible to design a phase gradient metasurface with a wide frequency band. To design a metasurface with a narrow band, the unit that forms the metasurface should have a strong resonant response (i.e., a high Q). To extend the anomalous reflection bandwidth of the phase gradient metasurface, we design and propose a cross-shaped unit, as shown in Fig. 1a, b. From the front view of the unit, it is shown that the unit is a square structure and the unit length is $a = 8.5$ mm. The geometrical dimensions of the element are mainly determined by the parameters $b1$, l, g, $w1$ and $w2$. Where $b1$ is the length of the cross metal wire, $r = l - w2/2$ is the radius of the inner ring, g is the gap size of the ring, $w1$ is the line width of the cross-shaped metal wire, and $w2$ is the line width of the opening ring. In the side view of the unit, it is shown that the unit consists of a three-layer structure: the upper layer is a cross-shaped metal foil layer with a thickness $t1 = 0.035$ mm. The dielectric constant of the intermediate dielectric layer is $\varepsilon_r = 2.65$, the loss tangent is $\tan\delta_r = 0.002$, and the thickness of the dielectric layer is $h = 3$ mm. The lower layer is a metal ground plane with a thickness $t1 = 0.035$ mm to provide the total reflection effect of the electromagnetic wave. As can be seen from Fig. 1c, d, the unit has the same electromagnetic properties for vertically incident TE and TM waves, and is shown to be polarization insensitive. The unit exhibits dual resonance characteristics across 8.0–20.0 GHz as is shown in Fig. 1c. Thus, the variation of reflection phase of the unit with frequency becomes stable across the two resonance points. Next we can use the calculation method of [26] to calculate the equivalent impedance of the surface. In the direction

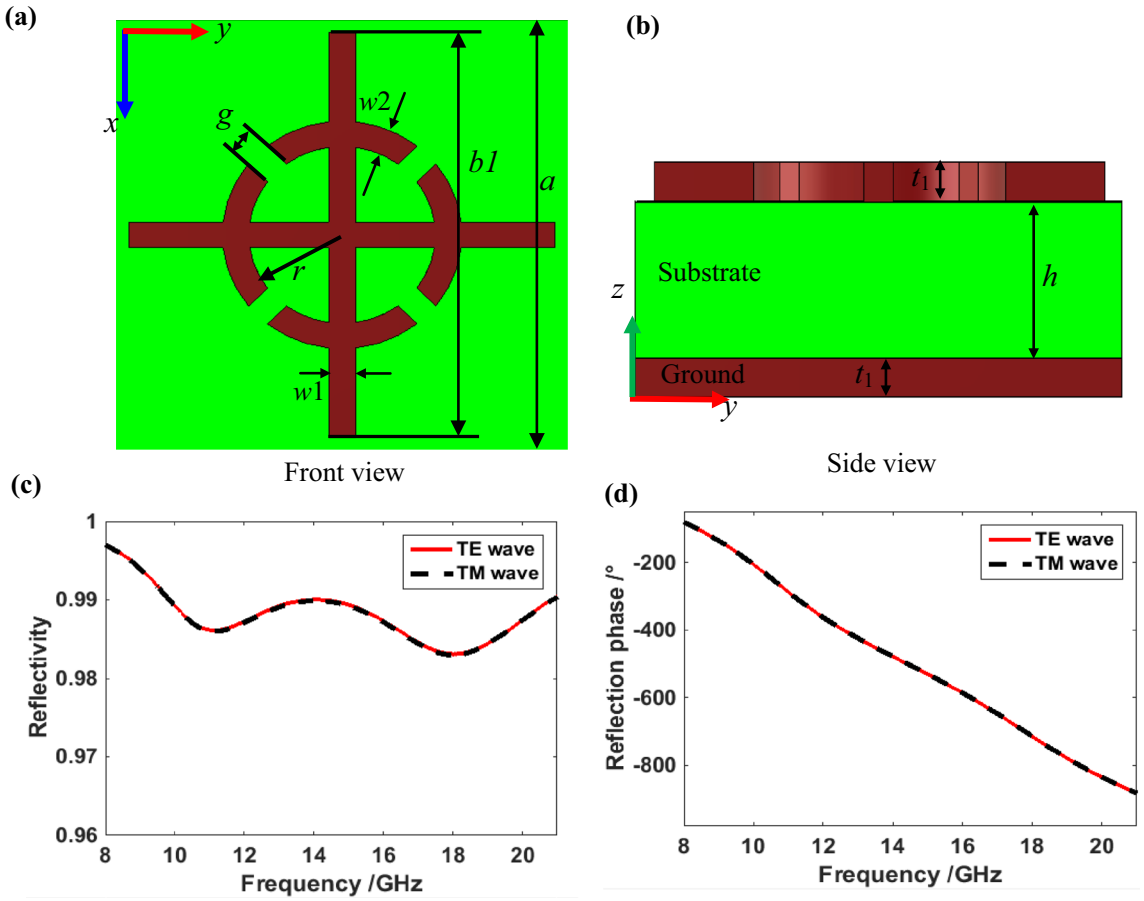

Fig. 1 The cross - shaped unit structure and simulation results. **a** The cross-shaped unit front view and **b** side view. **c** Reflectivity and **d** reflection phase of the element under the vertical incidence of TE and TM waves

of the axis coordinate, the metal layer can be equivalent to the equivalent circuit with the equivalent inductance L and the equivalent capacitance C connected in series. The corresponding equivalent impedance is $Z_s = j\omega L + 1/j\omega C$, and the phase of the reflection can be obtained by introducing Z_s into Eq. (1).

To design a metasurface with a phase gradient, we need to select a unit with a fixed reflection phase difference. It can be seen from Eq. (1) that the equivalent capacitance C and the equivalent inductance L of the unit structure change when the geometrical parameters of the metal element are changed, and the reflection phase of the metal element can be changed. After adjusting the geometric parameters $b1$, l, g, $w1$ and $w2$ of the unit, we select seven optimal units with different reflection phases. The size parameters of $b1$, l, g, $w1$ and $w2$ are : (1) $b1 = 5.5$, $g = 1.2$, $l = 1.6$, $w1 = 0.5$, $w2 = 0.4$, (2) $b1 = 6.5$, $g = 1.2$, $l = 1.5$, $w1 = 0.4$, $w2 = 0.8$, (3) $b1 = 7.0$, $g = 0.8$, $l = 1.75$, $w1 = 0.4$, $w2 = 1.2$, (4) $b1 = 6.5$, $g = 1.2$, $l = 2.5$, $w1 = 0.5$, $w2 = 1.0$, (5) $b1 = 6.5$, $g = 1.2$, $l = 2.5$, $w1 = 0.2$, $w2 = 1.2$, (6) $b1 = 7.0$, $g = 0.4$, $l = 2.75$, $w1 = 0.3$, $w2 = 0.8$, (7) $b1 = 8.0$, $g = 0.2$, $l = 2.75$, $w1 = 0.2$, $w2 = 0.8$, length units are mm. The reflectivity and reflection phase of the seven units are shown in Fig. 2, where Fig. 2a shows the relationship between the reflectance of seven different size parameter units with frequency and Fig. 2b shows the relationship between the reflection phase of seven units of different size with frequency. From the simulation results it can be seen that in the 8.0–20.0 GHz frequency range, each unit reflectivity is higher than 97%, the unit's energy loss is very small. The phase of the seven units can maintain a stable phase gradient distribution in most of the range of 8.0–20.0 GHz, and the phase shift of the element can satisfy the range of 2π.

We have analyzed the electromagnetic response of the unit whose size is $b1 = 8.0$, $g = 0.2$, $l = 2.75$, $w1 = 0.2$, $w2 = 0.8$, as shown in Fig. 3, where the direction of the incident electric field is in the x direction. As shown in Fig. 3, the electric field (shown in Fig. 3a), the magnetic field (shown in Fig. 3b) and electrical current (shown in Fig. 3c) on the unit surface distributes almost all through the top end cap to the bottom end cap at 10 GHz. When the frequency goes up to 18 GHz, the electric field (shown in Fig. 3d), the magnetic field (shown in Fig. 3e) and electrical current (shown in Fig. 3f) concentrates on the left end cap and the right end cap. The equivalent length of field distribution zone along incident electric field polarization direction (The E_x direction in Fig. 3) decrease. Thus, within the frequency range under consideration, the response size of the unit can approximately meet subwavelength conditions. By satisfying this condition, the phase of the reflection of the element can also achieve the 2π phase shift at high frequencies. According to this condition, we can design a metasurface with the broadband.

2.1.1 Design and analysis of wideband phase gradient metasurface with abnormal reflection

The generalized Snell reflection law points out that when a beam of electromagnetic waves irradiates on the surface with the incident angle θ_i, the difference of phase between the different propagation paths is zero. In addition, when there is a phase gradient at the interface and it is constant, here comes the generalized Snell's law of reflection [4]:

$$\sin\theta_r - \sin\theta_i = \frac{\lambda_0}{2\pi n_i} \cdot \frac{d\varphi}{dx}, \tag{2}$$

where θ_i is the angle of incidence, θ_r is the reflection angle, $d\varphi/dx$ is the phase delay caused by the two propagation paths adjacent on the surface, and λ_0 is the wavelength in vacuum. For two-dimensional artificial electromagnetic metasurface

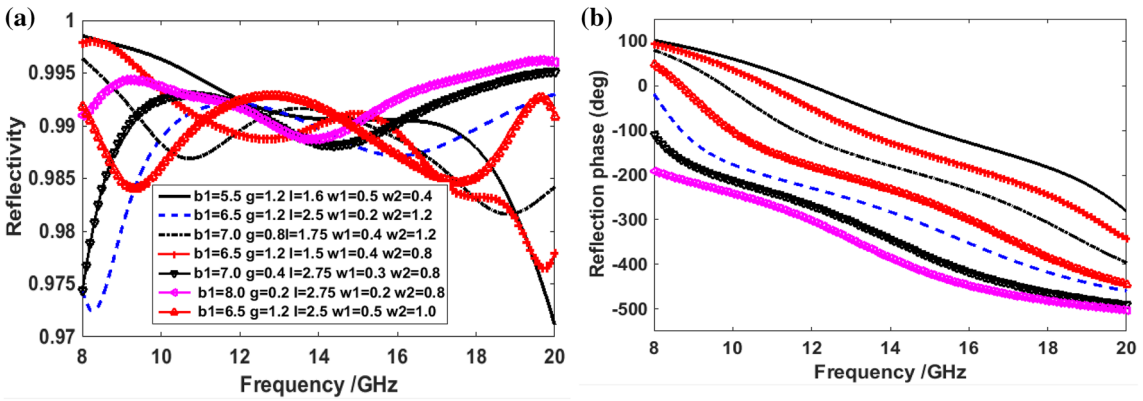

Fig. 2 **a** The reflectivity of the cross-shaped units of seven different sizes. **b** The reflection phase of the cross-shaped units of seven different sizes

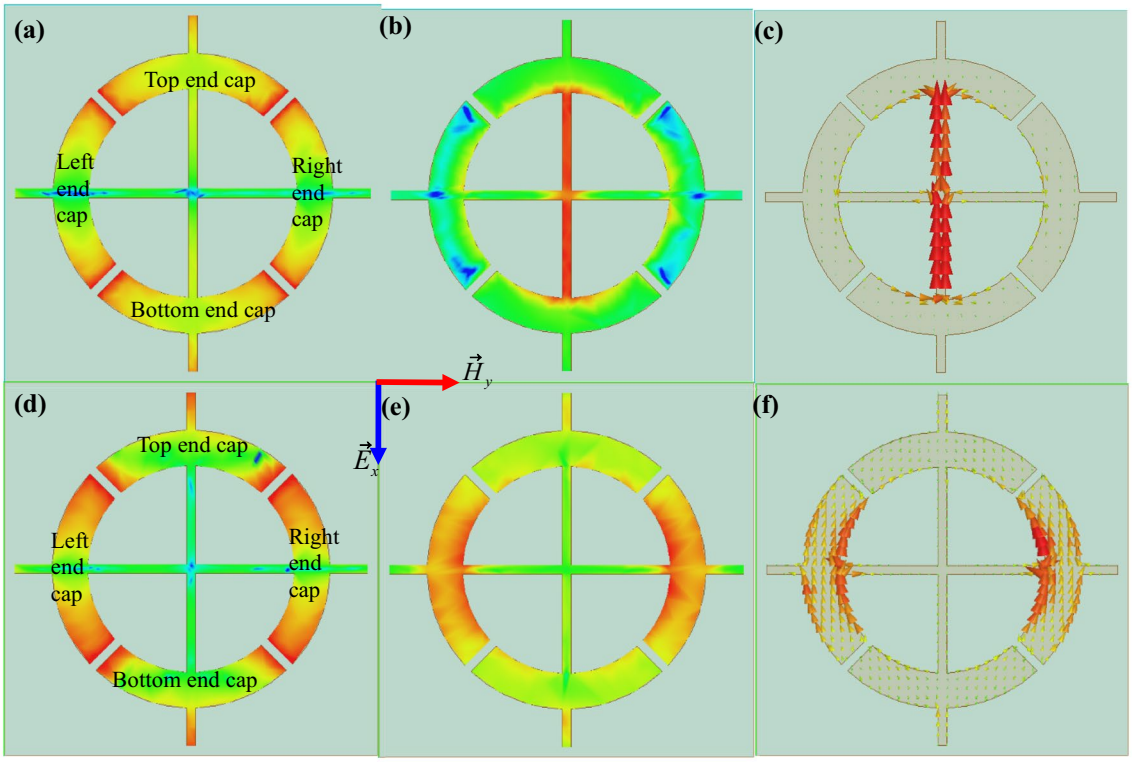

Fig. 3 **a**–**c** The distribution of the electric field, the magnetic field and the current at the surface of the element at 10.0 GHz. **d**–**f** The distribution of the electric field, the magnetic field and the current at the surface of the element at 18 GHz

composed of the discrete units with cyclical change, Then Eq. (2) can be simplified as:

$$\sin\theta_r - \sin\theta_i = \frac{\lambda_0}{aN}, \tag{3}$$

where a is the cycle size of the cell, N is the number of cells within the range of wavelength. When the electromagnetic wave irradiates on the surface vertically ($\theta_i = 0$), it is further simplified by Eq. (3):

$$\sin\theta_r = \frac{\lambda_0}{aN} \tag{4}$$

According to Eq. (3), the reflection angle θ_i is only related to the wavelength λ_0, a and N. At the frequency f_0, the deflection direction of the reflected beam can be changed only by changing the number of elements N and the unit period a in the metasurface to obtain the desired direction of reflection wave deflection.

According to the above method of phase gradient metasurface arrangement, seven units with different sizes are arranged in the x-axis and y-axis directions respectively, and the phase gradient metasurface is designed. Two neighbor cycles of the metasurface and their corresponding reflection phase gradient distribution are shown in Fig. 4. It can be seen that the phase difference between the last cell of the previous cycle and the first cell of the next cycle is 360°.

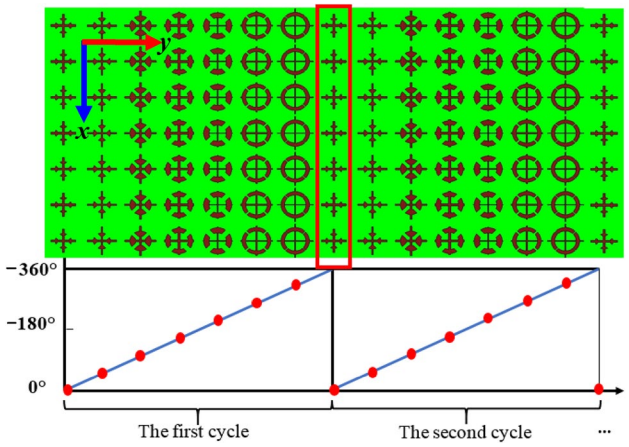

Fig. 4 Two neighbor cycles of the metasurface and their corresponding reflection phase gradient distribution

Next, we analyze the design of the phase gradient metasurface, and observe the reflection of the electromagnetic wave incident on the metasurface. According to the condition of $\theta_i = 0$ in Eq. (3), we use the vertically incident TE wave as the incident wave to simulate the designed metasurface, and

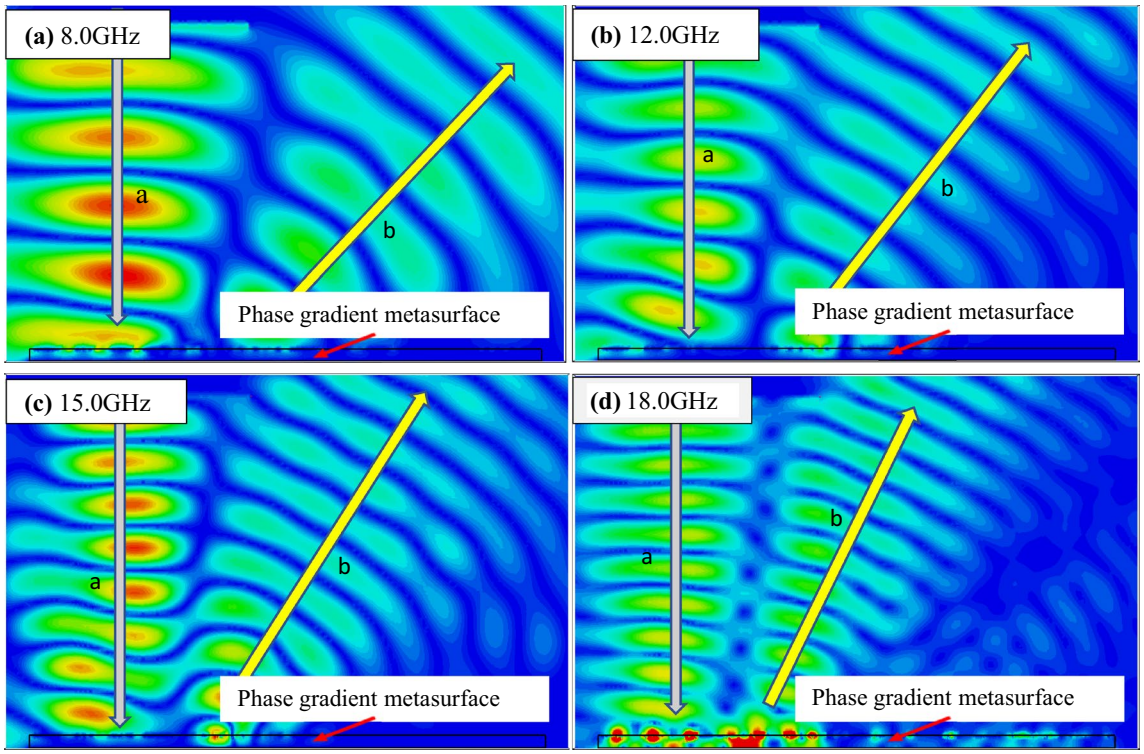

Fig. 5 Reflective state of incident electromagnetic wave on metasurface. **a–d** Are distributions of electromagnetic waves at 8.0, 12.0, 15.0, 18.0 GHz in the back-to-space of metasurface

obtain the path distribution of the reflected wave in the back-to-space region. As shown in Fig. 5a–d are the reflections of the electromagnetic waves of 8.0, 12.0, 15.0, and 18.0 GHz in the back-to-space of the metasurface. It is clear from the four figures that the propagation path of the incident electromagnetic wave and the reflected electromagnetic wave is clearly distinguished (where the gray arrow a represents the incident wave and the yellow arrow b represents the reflected wave). There is a certain angle between the incident electromagnetic wave and the reflected electromagnetic wave, indicating that the electromagnetic wave incident on the metasurface has an anomalous reflection phenomenon at the surface. It can also be seen that the angle between the incident and the reflected propagation path of the reflected electromagnetic wave is different at different frequencies.

To show the anomalous reflection phenomenon of the incident electromagnetic wave on the metasurface, we give the three-dimensional far-field energy pattern formed on the metasurface of the 28 × 28 elements (238 mm × 238 mm). As shown in Fig. 6a–d are three-dimensional far-field patterns with frequencies of 8.0, 12.0, 15.0 and 18.0 GHz, respectively. It can be seen from the four far field patterns that the propagation direction of the reflected wave produces different deflection angles and the effect of abnormal reflection is better. Figure 6e is the normalized two-dimensional far-field energy distribution on the *YZ* plane with the frequency $f = 15.0$ GHz. It can be seen from the figure that the reflected wave energy reaches the maximum at $\theta = 19.6°$, indicating that the anomalous deflection angle of the reflected wave is 19.6° and coincides with the theoretical deflection angle. Since the designed metasurface has a phase gradient in the *y*-axis direction, the wave vector of the reflected wave is generated in the *y*-axis direction so that the propagation direction of the reflected wave has a certain deflection angle in the + *y*-axis direction. At the same time, since the metasurface phase gradient is sufficient to control the propagation direction of the electromagnetic wave, the back reflection of the metasurface is small. In addition, it can be seen in Fig. 6 that the deflection angle of the reflected wave decreases gradually with increasing frequency. We then analyze the size of the deflection angle of reflected wave.

Figure 7 shows the relationship between the energy distribution deflection angle of the reflected wave and the frequency. Figure 7a shows the relationship between the energy distribution of reflected wave and the frequency. Figure 7b shows the relationship between the deflection angle of the reflected wave and the frequency. As can be seen from the two figures in Fig. 7, the energy of the reflected wave has a certain angular deflection in the frequency range, and the deflection angle decreases with increasing frequency. We can explain by Eq. (4), because the number of metasurface unit *N* and the unit

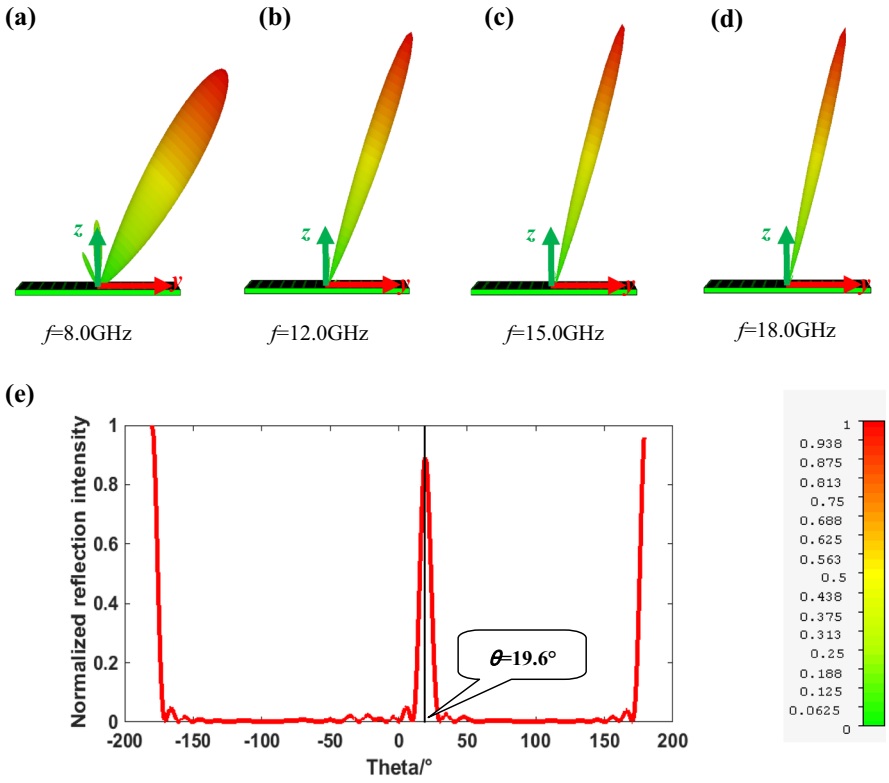

Fig. 6 The far-field pattern of the metasurface of the 28 × 28 elements consisting of the new cross-shaped element at different frequencies. **a**–**d** The three-dimensional pattern of the metasurface when the frequencies are 8.0, 12.0, 15.0, 18.0 GHz, respectively. **e** Normalized two-dimensional far-field energy distribution on the *YZ* plane when 15 GHz

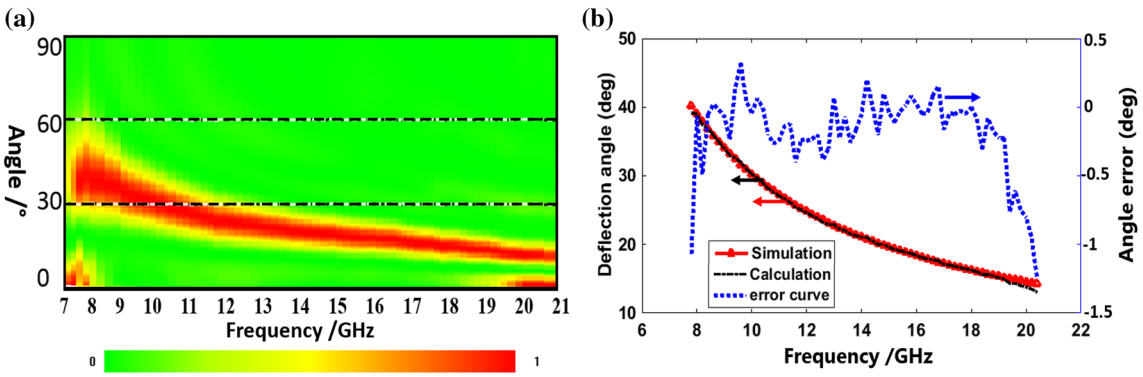

Fig. 7 **a** The relationship between the deflection angle of the reflected wave and the frequency. **b** The simulation value of the deflection angle of the reflected wave, the theoretical value and the error between the two

cycle size a has been determined, the deflection angle φ of reflected wave in the equation is only related to the wavelength of the electromagnetic wave λ. When studying the changes of deflection angle of reflected wave with frequency, the frequency is a variable, so the wavelengths λ are different at different frequency, resulting in the difference of deflection angle of reflected wave. Figure 7b is the theoretical result and simulation result of the deflection angle of the reflected wave. The black solid line represents the theoretical result. The red "△" line represents the simulation result, and the blue dotted line represents the error between the two. In the figure, we can see that the theoretical result is basically the same as the simulation result in the frequency range of 8.0–20.0 GHz, and the error between them is between − 1.5° and 0.5°. This shows that the design of the phase gradient metasurface is completely in accordance with the generalized Snell's law, and has a very good directional directionality.

3 Conclusion

We propose a cross-shaped unit with low Q value, analyze the electromagnetic response characteristics of the units at high frequency and low frequency, and give the reason of generating broadband. We use seven units with different reflection phases to design the phase gradient metasurface. Since there is only a phase gradient in the y direction, the reflected wave has a wave vector component in the y-axis direction, resulting in deflection of the reflected wave. From the simulation results, the design of the metasurface has a very good control effect on the reflected wave. Due to the design flexibility of the metasurface, the two axial parameters of the cell can also be designed separately to achieve separate modulation of the different polarized electromagnetic waves on the metasurface. This wideband metasurface can be used in the millimeter-wave or optical imaging, satellite communications, radar detection and so on, to improve the device bandwidth.

References

1. D.R. Smith, J.B. Pendry, M.C. Wiltshire. Science. **305**, 788–792 (2004)
2. R.W. Ziolkowski, E. Heyman, Phys. Rev. E Stat. Nonlinear Soft Matter Phys. **64**(2), 056625 (2001)
3. H. Cory, C. Zach, Microw. Opt. Technol. Lett. **40**(6), 460–465 (2004)
4. N. Yu, P. Genevet, M.A. Kats, F. Aieta, J.-P. Tetienne, F. Capasso, Z. Gaburro, Science. **334**, 6054:333–337 (2011)
5. F. Qin, L. Ding, L. Zhang, F. Monticone, C.C. Chum, J. Deng, S. Mei, Y. Li, J. Teng, M. Hong, S. Zhang, A. Alù, C. Qiu. Sci. Adv. **2**(1), e1501168 (2016)
6. H. Shi, J. Li, A. Zhang, Y. Jiang, J. Wang, Z. Xu, S. Xia. IEEE Antennas Wirel Propag. Lett. **14**, 104–107 (2015)
7. C. Huang, W. Pan, X. Ma, X. Luo, Sci. Rep. **6**, 23291 (2016)
8. X. Ding, F. Monticone, K. Zhang, L. Zhang, D. Gao, S.N. Burokur, A. de Lustrac, Q. Wu, C.W. Qiu, A. Alù, Adv. Mater. **27**(7), 1195–1200 (2015)
9. S. Sun, Q. He, S. Xiao, Q. Xu, X. Li, L. Zhou, Nat Mater. **11**(5), 426–431 (2012)
10. H.L. Zhu, S.W. Cheung, K.L. Chung, T.I. Yuk, IEEE Trans. Antennas Propag. **61**(9), 4615–4623 (2013)
11. X. Ding, H. Yu, S. Zhang, Y. Wu, K. Zhang, Q. Wu, IEEE Trans. Magn. **51**(11), 1–1 (2015)
12. F. Aieta, P. Genevet, M.A. Kats, N. Yu, R. Blanchard, Z. Gaburro, F. Capasso. Nano Lett. **12**(9), 4932–4936 (2012)
13. Y. Zhang, L. Liang, J. Yang, Y. Feng, B. Zhu, J. Zhao, T. Jiang, B. Jin, W. Liu, Sci. Rep. **6**, 26875 (2016)
14. K. Chen, Y. Feng, Z. Yang, L. Cui, J. Zhao, B. Zhu, T. Jiang, Sci. Rep. **6**, 35968 (2016)
15. J. Su, Y. Lu, H. Zhang, Z. Li, Y. Yang, Y. Che, K. Qi. Sci. Rep. **7**, 42283 (2017)
16. H. Sun, C. Gu, X. Chen, Z. Li, L. Liu, B. Xu, Z. Zhou, Sci. Rep. **7**, 40782 (2016)
17. C.L. Holloway, E.F. Kuester, J.A. Gordon, J. O'Hara, J. Booth, D.R. Smith. IEEE Antennas Propag. Mag. **54**(2), 10–35 (2012)
18. Y. Jang, M. Yoo, S. Lim, Opt. Express. **21**(20), 24163 (2013)
19. N. Meinzer, W.L. Barnes, I.R. Hooper, Nat Photonics. **8**, 889–898 (2014)
20. X. Ni, N.K. Emani, A.V. Kildishev, A. Boltasseva, V.M. Shalaev, Science. **335**(6067), 427 (2012)
21. Y. Li, J. Zhang, S. Qu, J. Wang, H. Chen, L. Zheng, Z. Xu, A. Zhang, J.Phys. D Appl. Phys. **47**(42), 425103–425109 (2014). 7)
22. S. Kruk, B. Hopkins, I.I. Kravchenko, A. Miroshnichenko, D.N. Neshev, Y.S. Kivshar, APL Photonics. **1**(3), 030801 (2016)
23. Y. Yang, W. Wang, P. Moitra, I.I. Kravchenko, D.P. Briggs, J. Valentine, Nano Lett. **14**(3), 1394–1399 (2014)
24. Y.F. Yu, A.Y. Zhu, R. Paniagua-Domínguez, Y.H. Fu, B. Luk'yanchuk, A.I. Kuznetsov Laser Photonics Rev. **9**(4), 412–418 (2015)
25. S. Sun, K. Yang, C. Wang, T.-K. Juan, W. Chen, C. Liao, Q. He, S. Xiao, W. Kung, G. Guo, L. Zhou, D. Ping Tsai, Nano Lett. **12**(12), 6223–6229 (2012)
26. M. Pu, P. Chen, C. Wang, Y. Wang, Z. Zhao, C. Hu, C. Huang, X. Luo, Aip Adv. **3**(5), 77 (2013)
27. H.F. Ma, Y.Q. Liu, K. Luan, T.J. Cui, Sci. Rep. **6**, 39390 (2016)
28. X. Luo, Sci. China Phys. Mech. Astron. **58**, 594201 (2015)